Numerical investigation of regimes of current transfer to anodes of high-pressure arc discharges

D. F. N. Santos[1,2], N. A. Almeida[1,2], M. Lisnyak[3], J.-P. Gonnet[3], and M. S. Benilov[1,2,4]

[1]Departamento de Física, Faculdade de Ciências Exatas e da Engenharia, Universidade da Madeira, 9000 Funchal, Portugal

[2]Instituto de Plasmas e Fusão Nuclear, Instituto Superior Técnico, Universidade de Lisboa, 1049-001 Lisboa, Portugal

[3]Schneider Electric Science and Technology, 38050 Grenoble Cedex 9, France

[4]Corresponding author. E-mail: *benilov@staff.uma.pt*

Abstract

The unified 1D numerical modelling of high-pressure high-current arc discharges is revisited. Two regimes of current transfer to anodes are investigated. The "passive anode" regime occurs for low and moderate anode surface temperatures T_a. The energy flux from the plasma to the anode surface, q_{pl}, depends on T_a rather weakly in this regime and may be conveniently expressed in terms of the local current density j_c and the so-called anode heating voltage U_h. U_h is independent of the arc length and the cathode surface temperature, although it weakly varies with j_c, between approximately 6 and 8.5 V for j_c in the range from 10^5 to 10^8 A m^{-2}. In the "active anode" regime, q_{pl} is higher than in the passive anode regime and varies with T_a. The active anode regime may occur on hot refractory anodes, such as those of high-intensity discharge lamps, when T_a exceeds approximately 3000 K and the thermionic electron emission from the anode comes into play. The latter causes an increase in the electron density near the anode. One consequence is an increase of the electron energy transport from the bulk plasma to the near-anode layer by electron heat conduction. The other effect contributing to increase of q_{pl} is the formation of a negative near-anode space-charge sheath with a positive voltage drop. In non-stationary simulations, the active regime occurs via the development of a thermal instability, similar to that causing appearance of spots on thermionic arc cathodes. The occurrence of the active regime is strongly affected by parameters, in particular, by the distance between the anode surface and the cooling fluid.

1 Introduction

Electrode phenomena play a key role in the physics of high-pressure arc discharges and electrodes are often the limiting component in plasma arc technology. Reviews on this topic have recently been published at a fairly high rate [1–12]. Near-cathode and near-anode phenomena in high-pressure arc discharges are manifestly different. In particular, the near-anode voltage

drop is usually smaller than the near-cathode voltage drop and can be both positive and negative. It is said sometimes that the anode plays a more passive role in the arc physics than the cathode; e.g., the book [8]. However, the physics of current transfer to the anodes is by no means simple, especially for high arc current, when the arc attachment to the anode is affected by cathode jets, and it can be diffuse or constricted, and a severely constricted anode attachment (spot) creates a pumping action that results in the formation of an anode jet. Reviews of the literature dedicated to the interaction of the high-pressure arc plasma with the anodes can be found in [3–5].

There is a large number of papers devoted to various aspects of the theory and modeling of the interaction between high-pressure arc plasmas and electrodes, many of them published recently; e.g., reviews [11, 12]. Still, the modelling of arc-electrode interaction remains a non-trivial task due to a wide variety of physical mechanisms that are difficult to account for in the same framework. In particular, near-electrode space-charge sheaths in high-current arcs are difficult to simulate beyond the one-dimensional (1D) approximation, while cathode jets are a multidimensional phenomenon. By now, most of the modelling of arc-anode interaction has been performed in the 1D approximation, following the classic work [13]. 1D modelling does not self-consistently describe phenomena in the arc bulk. Nonetheless, useful results have been obtained, in particular, on ablating anodes; e.g., [14–16].

A natural way to develop a numerical model that would take into account all mechanisms affecting current transfer to the anodes of high-current arcs is to use a multidimensional MHD model of the arc bulk, formulated under an appropriate approximation, for example, the approximation of local thermodynamic equilibrium (LTE), and supplement it with boundary conditions at the anode surface describing the physics of the non-equilibrium near-anode layer. (More precisely, the boundary conditions apply at the edge of the non-equilibrium near-anode layer; however, this 'edge' coincides with the anode surface when considered on the length scale of the bulk plasma.) MHD arc modeling under the LTE approximation is now a matter of routine and can be used to simulate cathode and anode jets, arc constriction *etc.* On the other hand, the formulation of practical and physically justified boundary conditions at the anode surface, which would reasonably accurately describe the near-anode physics, remains a challenging task.

One of the necessary boundary conditions at the anode surface concerns the energy flux from the plasma to the surface. This condition may be formulated as follows. It is known from the experiment that the power input Q from high-pressure arc plasma to the anode of a low-current high-pressure arc, such as those used in high-intensity discharge (HID) lamps, is approximately proportional to the arc current I:

$$Q = IU_h, \tag{1}$$

where U_h is a proportionality coefficient, called the volt equivalent of the heat flux to the anode or the anode heating voltage. U_h may depend on the plasma-producing gas and its pressure and on the work function of the anode material, but not on the arc current, nor on the anode surface temperature, nor on the anode design. For example, experiments [17], performed with thin tungsten rod electrodes of different dimensions in a 2.6 bar Ar arc, gave $U_h = 6.2\,\mathrm{V}$ [4].

Eq. (1) involves integral parameters of the arc, rather than local parameters (parameters at each point of the anode surface), which are relevant to multidimensional arc models. Moreover, the experiment [17], where this equation was established, has been performed at arc currents not exceeding approximately 5 A. Therefore, Eq. (1) cannot be directly used in multidimensional

modelling of high-current arcs. On the other hand, one can use a local version of this equation,

$$q_{pl} = j_c U_h, \tag{2}$$

where q_{pl} is the density of the energy flux from the plasma to the anode surface and j_c is the density of electric current from the anode surface into the plasma. Relation (2) was derived from the 1D modelling of near-anode layers of high-pressure arc discharges [18], performed for three plasma-producing gases (Ar, Xe, and Hg) in a wide range of current densities j_c, anode surface temperatures T_a, and plasma pressures p. In particular, the proportionality coefficient U_h derived for argon for $10^6\,\mathrm{A\,m^{-2}} \le j_c \le 10^7\,\mathrm{A\,m^{-2}}$, $300\,\mathrm{K} \le T_a \le 3000\,\mathrm{K}$, and $1\,\mathrm{bar} \le p \le 10\,\mathrm{bar}$ was approximately 6 V, in close agreement with the experimental value cited above.

Note that in the model [18] the major contribution to the energy released at the anode per electron, which in this example equals 6 eV, is given by the electron condensation heat. The latter equals the work function of the anode material; 4.5 eV in the modelling [18]. This suggests a simple physical picture: the near-anode region does not significantly contribute to the heating of the anode, only ensuring that the anode collects the right amount of electrons to maintain the current continuity. Therefore, the regime of the current transfer to the anodes of high-pressure arc discharges where the Eq. (2) holds may be called a "passive anode" regime.

Eq. (2) represents a convenient boundary condition for models with an MHD description of the arc bulk. For example, this equation with $U_h = 6\,\mathrm{V}$ was used in [19] to formulate a boundary condition on the surface of anode of a 1 cm-long free-burning atmospheric-pressure argon arc in the framework of a numerical model based on a two-dimensional MHD LTE description of the arc bulk. However, there are limitations. The computation domain in the modelling [18] was the near-anode non-equilibrium plasma layer bordering an LTE arc column. This implies that the arc bulk is in the state of LTE. However, the latter may not be the case if the arc too short and/or the arc current is too low. The question is if Eq. (2) remains applicable in the whole range of arc lengths and arc currents where the arc bulk is still close to LTE. Another important question is whether the value $U_h = 6\,\mathrm{V}$ is suitable in the whole range of parameters where Eq. (2) remains applicable.

A further question is whether the passive anode regime is the only one theoretically possible; it may be that other regimes are possible as well but have not been detected in the numerical modelling. Note that, within the framework of this work, different regimes of current transfer to the anodes of high-pressure arc discharges differ from each other by the mechanisms of plasma heating of the anode (and not by positive or negative near-anode voltage, as in the previous numerical studies [14, 20, 21]). Thus, the above question amounts to whether anode operation regimes are possible where the energy flux density to the surface is not proportional to the local current density.

In this work, the 1D non-equilibrium numerical modelling of current transfer to electrodes of high-pressure arc discharges is revisited. To answer the above questions, the computational domain includes the entire arc from the cathode to the anode. It is found that Eq. (2) remains applicable under all conditions where the LTE modelling approach as such is justified, that is, in the case when the arc length and current are high enough so that the plasma in the arc bulk is close to LTE. The value of U_h is independent of the arc length and of the cathode surface temperature, although it weakly varies with the current density j_c, between approximately 6 and 8.5 V for j_c in the range from 10^5 to $10^8\,\mathrm{A\,m^{-2}}$. The values of U_h found for short arcs and low arc current densities, where the arc bulk is far away from the LTE state, may be viewed as a convenient form of presentation of results of non-equilibrium modelling of the entire

interelectrode gap. It is found also that, in addition to the passive anode regime described by Eq. (2), another regime is possible, which may occur on hot refractory anodes, such as the electrodes of HID lamps. The energy flux to the anode surface, q_{pl}, in this regime first increases with increasing anode surface temperature T_a and then, depending on conditions, may begin to decrease. The increasing dependence $q_{pl}\left(T_a\right)$ can cause thermal instability, similar to that resulting in the appearance of spots on thermionic arc cathodes.

The outline of the paper is as follows. The numerical model is described in Sec. 2. Modelling results are reported and discussed in Secs. 3-7. Conclusions are given in Sec. 8.

2 Numerical model

The numerical model is based on the so-called unified modelling approach [22–37], where the single set of differential equations, comprising conservation and transport equations for all plasma species, the electron and heavy-particle energy equations, and the Poisson equation, is solved in the whole interelectrode gap up to the electrode surfaces. The strengths and weaknesses of this approach have been discussed elsewhere [36]. Here we only stress that there is no need in the framework of the unified approach to a priori theorize about dominating physical mechanisms for different parameter ranges in different plasma regions, such as LTE bulk plasma and non-equilibrium near-electrode layers. Rather, dominating physical mechanisms are seen in the modelling results.

The unified modelling is computationally intense and its application has been limited to one-dimensional (1D) situations, except in cases of very low current density. 1D modelling does not self-consistently describe phenomena in the arc bulk. However, it reasonably accurately describes phenomena in thin non-equilibrium near-electrode plasma layers and thus is sufficient for the purposes of this work.

We consider the ignition of a discharge in a cold atomic gas between two parallel electrodes with a subsequent transition to a steady-state arc discharge. The pressure is atmospheric. The computation domain is shown in Fig. 1. $0 < x < h$ is the plasma domain, $-h_1 \le x \le 0$ and $h \le x \le h + h_2$ are the electrodes. Here h, h_1, and h_2 are given parameters having the meaning of, respectively, the arc length, the cathode height (the distance from the cathode surface to the cooling fluid), and the anode height.

The system of equations is written in the 1D non-stationary form. Equations in the plasma include the species conservation and transport equations, the heavy-particle and electron energy equations, and the Poisson equation. The species taken into account are the neutral particles (atoms), the singly charged ions, and the electrons; the effect of the excited atoms is taken into account in terms of stepwise ionization/recombination. The transport equations are written in the form of the Stefan-Maxwell equations. The heat conduction equations are solved inside the electrodes. The equations and the boundary conditions are written in the spirit of previous works [22, 25, 29, 36] and are the same as those used in [36]. Note that there is a formatting error in the second term on the rhs of Eq. (17) of [36], which is the equation of the heavy-particle energy; the correct form of this term is $\frac{p_h}{\rho}\frac{d\rho}{dt}$. While being discarded in the modelling [36], this term was taken into account in the modelling of this work.

For the purposes of this work, it is convenient to explicitly write some of the boundary conditions applied in the model on the electrode surfaces. The boundary condition for the density of the electrons is given by an equation of particle balance at the electrode surface; cf.

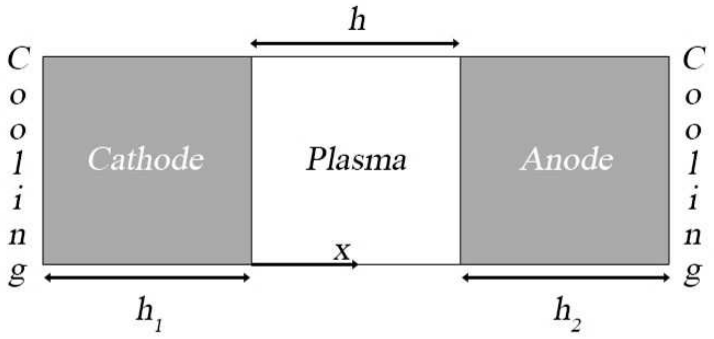

Figure 1. Schematic of calculation domain.

Eq. (3) of [36]:

$$J_e = n\left(\frac{j_{em}}{e} - \frac{j_{cd}}{e}\right). \tag{3}$$

Here J_e is the projection onto the x-axis of the vector of the density of transport flux of the electrons; $n = 1$ for $x = 0$ and $n = -1$ for $x = h$; j_{em} is the density of electron emission current; and j_{cd} is the density of current of electrons coming to the electrode surface from the plasma. j_{cd} is written as

$$j_{cd} = \frac{en_eC_e}{4}, \tag{4}$$

where n_e is the electron number density and C_e is the mean speed of random motion of the electrons. C_e is defined by the conventional formula $C_e = (8kT_e/\pi m_e)^{1/2}$, where T_e is the electron temperature, k is the Boltzmann constant, and m_e is the electron mass.

The boundary condition for the electron energy is given by an equation of balance of energy at the electrode surface; cf. Eqs. (7) and (21) of [36]:

$$q_e = n\left(j_{em}\frac{2kT_s}{e} - j_{cd}\frac{2kT_e}{e}\right). \tag{5}$$

Here q_e is the projection onto the x-axis of the vector of the density of flux of thermal energy of the electrons and T_s is the temperature of the electrode body. q_e is written as

$$q_e = q_{e1} + q_{e2} + q_{e3}, \tag{6}$$

where q_{e1}, q_{e2}, and q_{e3} are components of the density of the electron thermal energy flux due to, respectively, the enthalpy transport by the electron transport flux, the heat conduction, and the effect inverse to the thermal diffusion. q_{e1} and q_{e2} are written as

$$q_{e1} = \frac{5}{2}kT_eJ_e, \quad q_{e2} = -\kappa_e\frac{\partial T_e}{\partial x} \tag{7}$$

(κ_e is thermal conductivity of the electron gas), q_{e3} is given by the last term on the rhs of Eq. (15) of [22].

Another boundary condition is the condition of continuity of the energy flux at the electrode surface; cf. Eq. (10) of [36]:

$$q_{pl} = q_s. \tag{8}$$

Here q_{pl} is a projection onto the x-axis of the vector of the density of the net energy flux transported to the electrode surface from the plasma side, except for radiation; and q_s is a projection onto the x-axis of the vector of the density of the energy flux removed from the surface by heat conduction into the body of the electrode and by radiation.

q_{pl} is written as

$$q_{pl} = q_h + q_e + A_f J_e + (A_i - A_f)\, J_i, \tag{9}$$

where q_h is the projection onto the x-axis of the vector of the density of flux of thermal energy of the heavy particles; J_i is the projection onto the x-axis of the vector of the density of transport flux of the the ions; A_f is the work function; and A_i is the ionization energy of plasma-producing gas (15.76 eV for argon). q_h is written in the conventional form $q_h = -\kappa_h\, \partial T_s/\partial x$, where κ_h is the thermal conductivity of the heavy particle gas. The term $A_f J_e$ on the rhs of Eq. (9) accounts for cooling or heating of the electrode surface by the electron flux due to, respectively, electron emission or condensation. The term $(A_i - A_f)\, J_i$ accounts for the energy released at the electrode surface due to the neutralization of the ions.

Note that cooling of the electrode surface due to evaporation of the electrode material is neglected in Eq. (9). This effect was analyzed in [38] and the conclusion was that for atmospheric-pressure arcs this effect is minor while the electrode surface temperature is below the boiling point, but may come into play at higher temperatures. Given the importance, this point was revisited in Appendix A, with the same conclusion.

q_s is written in the conventional form

$$q_s = -\kappa_s \frac{\partial T_s}{\partial x} + \varepsilon \sigma T_s^4, \tag{10}$$

where κ_s is the thermal conductivity of the electrode material; ε is the hemispherical total emissivity of the electrode surface; and σ is the Stefan-Boltzmann constant. The terms on the rhs account for the losses of energy of the electrode surface due to, respectively, the heat conduction into the body of the electrode and thermal radiation from the surface into the plasma. Note that test simulations performed without account of the thermal radiation losses have revealed a quantitative change of results in the range of T_s high enough, but no qualitative changes. For this reason, Eq. (10) does not account for the heating of the electrode surface due to absorption of the radiation coming from the plasma, which may be of the same order of magnitude as the radiation losses [39], but is more difficult to evaluate.

The density of electron emission current is determined as $j_{em} = j_{TF} + j_{se}$. Here j_{TF} is the density of electron emission current caused by high values of the electrode surface temperature and/or of the electric field (if the latter is directed to the electrode surface) and j_{se} is the density of secondary electron emission current. j_{TF} is evaluated in the same way as in [36]: with account of field to thermo-field to thermionic emission mechanisms or only thermionic emission mechanism, depending on whether the local electric field is directed from the plasma to the electrode surface or in the opposite direction. j_{se} is evaluated as $j_{se} = e\gamma\,|J_i|$ regardless of the electric field direction (in contrast to [36], where j_{se} was neglected in cases where the local electric field is directed from the electrode surface into the plasma). Here γ is the so-called effective secondary emission coefficient, which is assumed to characterize all mechanisms of

secondary electron emission: due to ion, photon, and excited species bombardment; e.g., Sec. 4.7.2 of [40].

Note that the boundary condition for the density of the electrons (3), which describes balance of the electron particle fluxes on the electrode surface, does not expressly depend on the direction of the electric field at the electrode surface (although j_{em} does depend, as explained in the previous paragraph, and γ, in principle, can depend as well). However, this does not mean that all the electrons emitted by the electrode surface will go away from the surface into the plasma in all the cases: if the electric field is directed into the plasma, most of the emitted electrons will return to the surface as they should; e.g., Fig. 6(a) below.

The numerical method is the same as in [36]. The current density is treated as a known function of time, $j_c = j_c(t)$ (here j_c is the projection of the current density vector along the direction from anode to cathode). The temporal evolution of the discharge voltage $V_a(t)$ is computed.

Results reported in this work refer to arcs in argon under atmospheric pressure. The transport, kinetic, and radiation properties of the argon plasma are evaluated using formulas [22]. Cathode is made of tungsten. Anode materials of most interest are copper, of which massive water-cooled anodes are made, and tungsten, which is used for electrodes of HID lamps. The thermal conductivity of tungsten is taken from [41]. The emissivity of tungsten electrode surface is evaluated by means of the empirical equation (6.15) of [42] for $T_s \leq 3800\,\mathrm{K}$ and is set constant, $\varepsilon = 0.35$, for higher T_s. The thermal conductivity of copper is evaluated by means of the fit formula [43], which approximates the data [44]. (Note that most of the results for convenience are given in a form that does not depend on values of thermal conductivity of the anode material or is scalable with respect to these values.) The emissivity of a copper anode surface for $T_s \leq 1200\,\mathrm{K}$ is evaluated by means of the formula $\varepsilon = 0.013 + 2.22 \times 10^{-5} T_s/\mathrm{K}$, which was constructed on the basis of the data [44–47], and is set constant, $\varepsilon = 0.040$, for higher T_s. Values of the work function and the Richardson constant for the cathode surface are those given in the reference book [48] for tungsten: $4.5\,\mathrm{eV}$ and $0.60 \times 10^6\,\mathrm{A\,m^{-2}\,K^{-2}}$, respectively. Since these values are characteristic of many other metals including copper [49], they were used also for the anode surface.

Simulation results are reported for three values of the arc length h: $0.1\,\mathrm{mm}$, $1\,\mathrm{mm}$, and $10\,\mathrm{mm}$. (Note that arcs of submillimeter lengths occur, e.g., at initial stages of separation of the contacts of low-voltage circuit breakers. In addition, $h = 0.1\,\mathrm{mm}$ is a convenient test case to illustrate some of the effects that will be described in this work.) The effective secondary emission coefficient γ was set equal to 0.1, similarly to previous works [27, 31, 36]. The cathode height is $h_1 = 10\,\mathrm{mm}$ and the anode height h_2 is variable. The temperatures at the bottom of the cathode ($x = -h_1$) and anode ($x = h + h_2$) are controlled by external cooling and set equal to $300\,\mathrm{K}$.

3 Discharge ignition on cold electrodes in cold gas

An example of the computed temporal evolution of the discharge voltage V_a, the cathode surface temperature T_c, and the anode surface temperature T_a during discharge ignition on the cold electrodes in the cold gas is shown in Fig. 2(a) for various values of the anode height h_2. The simulations were initiated at $t = 0$, the current density linearly increases with time from 0 to $10^7\,\mathrm{A\,m^{-2}}$ within $1\,\mathrm{ms}$ and is maintained constant after $1\,\mathrm{ms}$. The discharge attains steady state on the time scale of seconds.

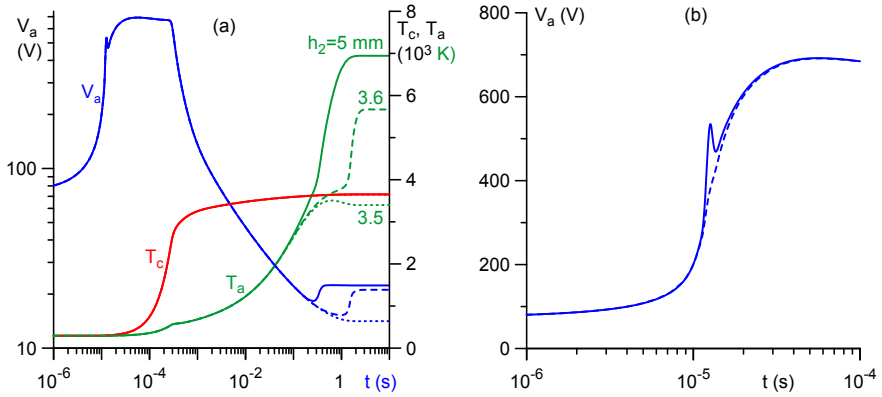

Figure 2. (a): evolution of the discharge voltage and electrode surface temperatures for different values of the anode height h_2. Solid: $h_2 = 5\,\mathrm{mm}$. Dashed: $3.6\,\mathrm{mm}$. Dotted: $3.5\,\mathrm{mm}$. (b): details of the evolution of the discharge voltage on the time scale $10^{-5}\,\mathrm{s}$, computed in two different approximations (see text), $h_2 = 5\,\mathrm{mm}$. $h = 0.1\,\mathrm{mm}$, $j_c = 10^7\,\mathrm{A\,m^{-2}}$.

Note that an appropriate choice of details of initial conditions depends on the way in which the simulated discharge is initiated (e.g., by the separation of contacts or an overvoltage). On the other hand, this point is not critical for the purposes of this work, since the effect of the details of the initial conditions is localized on sub-microsecond times [36]. The results reported in this work have been computed for the same initial conditions as those used in [36]: $n_i = n_e = 10^{16}\,\mathrm{m^{-3}}$, $T_h = T_s = 300\,\mathrm{K}$, $T_e = 20 \times 10^3\,\mathrm{K}$ (here n_i is the ion number density and T_h is the heavy-particle temperature).

There is a small oscillation in the discharge voltage at about $t = 10^{-5}\,\mathrm{s}$ for all values of the anode height. This oscillation is shown in detail by the solid line in the Fig. 2(b). It was found that this oscillation stems from the non-stationary term of the ion conservation equation. In this work, the non-stationary term was assumed in the form $\rho\frac{d(n_i/\rho)}{dt}$, cf. Eq. (13) of [36]. (Here ρ is the mass density of the plasma.) If this term is simplified to dn_i/dt, the oscillation disappears, as shown by the dashed line in Fig. 2(b). On the other hand, this peculiarity is irrelevant to the thermal regime of the anode, to which this work is devoted, and in any case, the rest of the modeling of this work is stationary. Therefore, this peculiarity was not investigated further.

The solid, dashed, and dotted lines in Fig. 2(a) are superposed for $t \lesssim 0.1\,\mathrm{s}$. In other words, there is virtually no effect of the anode height h_2 in this time range. As far as the cathode temperature is concerned, the effect remains virtually inexistent also for $t \gtrsim 0.1\,\mathrm{s}$. As far as the discharge voltage is concerned, the effect is visible: V_a increases with increasing h_2 for $t \gtrsim 0.1\,\mathrm{s}$. Note that the sign of the effect is somehow counterintuitive: an increase of the distance from the plasma to the cooling fluid amounts to a better thermal insulation of the discharge, which normally results in a lower, not higher, power necessary to support the same current.

The effect of variation of the anode height h_2 in the time range $t \gtrsim 0.1\,\mathrm{s}$ on the anode surface temperature T_a is very strong. For $h_2 = 3.5\,\mathrm{mm}$, the anode surface attains the temperature of approximately 3500 K in the steady state. In the case $h_2 = 3.6\,\mathrm{mm}$, it seems that the calculated temperature of the anode surface will reach a steady-state value of about 4000 K, but at $t \approx 1\,\mathrm{s}$

T_a starts rapidly increasing, apparently due to a thermal instability, and reaches a steady-state value of 5750 K. Note that the latter value is close to the boiling point of tungsten (5830 K); the evaporation cooling may play a role in the thermal balance of the anode, as discussed in Appendix A, and therefore the computation results may be at best qualitatively correct for temperatures that high. For $h_2 = 5$ mm, the computed stationary temperature of the anode surface is still higher, around 6900 K.

The above data have been obtained for the anode thermal conductivity $\kappa_s(T_s)$ equal to thermal conductivity of tungsten. Let us introduce the heat flux potential of the anode metal: $\psi(T_s) = \int_{T_{s2}}^{T} \kappa_s(T_s)\, dT$, where $\kappa_s = \kappa_s(T_s)$ is the thermal conductivity of the metal and T_{s2} is the temperature of the anode bottom (300 K). The value of the heat flux potential of tungsten for, e.g., $T_s = 6000$ K is approximately 5.5×10^5 W m^{-1}. A similar value for copper is approximately two times higher. It follows that, if the radiation cooling were unessential, then similar steady-state values of T_a for a copper anode would be achieved for h_2 approximately two times larger than those for tungsten. It can be shown that the account of radiation cooling changes this conclusion only slightly. However, one should not forget that the boiling point of copper is significantly lower than for tungsten: 2835 K.

Thus, in this example the increase of the distance from the plasma-anode interface to the cooling fluid from 3.5 mm to 3.6 mm for tungsten anode and from 6.5 to 7.0 mm for copper anode causes a dramatic increase of the computed stationary temperature of the anode surface, from 3500 K to 5750 K. There is a further rapid increase in the computed anode surface temperature as h_2 is increased to 5 or, respectively, 10 mm. We stress once again that the modelling is at best qualitatively correct for temperatures above the boiling point. On the other hand, surface temperatures above the boiling point will cause a fast destruction of the anode, if they occur in the experiment, and in this sense qualitative results are sufficient for practice. Thus, this is an interesting and potentially important phenomenon, which is studied in some detail in the next sections.

4 Stationary thermal balance of the anode

In Fig. 3, both sides of Eq. (8), evaluated at the anode surface for the steady-state conditions, are plotted as functions of the anode surface temperature T_a. The range of T_a values of up to 10^4 K is shown to illustrate the global pattern, but need not be reminded that computations for T_a values higher than the boiling point may be far from reality. The energy flux removed by heat conduction from the surface into the body of the anode and by thermal radiation into the plasma, q_s, which is shown by the solid lines, equals $\psi(T_a)/h_2 + \varepsilon\sigma T_a^4$ in the steady-state conditions, and was evaluated in terms of thermal conductivity and emissivity of tungsten. As mentioned above, similar values of q_s for copper are obtained for h_2 approximately two times larger. As an example, the dotted line in Fig. 3(a) depicts q_s for copper for $h_2 = 4.5$ mm. It is seen that the dotted line is indeed close to the solid line for $h_2 = 2$ mm.

The energy flux coming from the plasma to the anode surface, q_{pl}, which is shown by the dashed lines, was evaluated numerically with the anode body removed from the computation domain and the temperature of the anode surface, T_a, being a control parameter. Note that while the solid lines in Figs. 3(a) and (b) are the same (except that not all h_2 values are the same), the dashed lines are different.

For the solution to self-consistently describe stationary states of the arc (considered jointly with the cathode) and the anode, the boundary condition (8) must be satisfied. In other words,

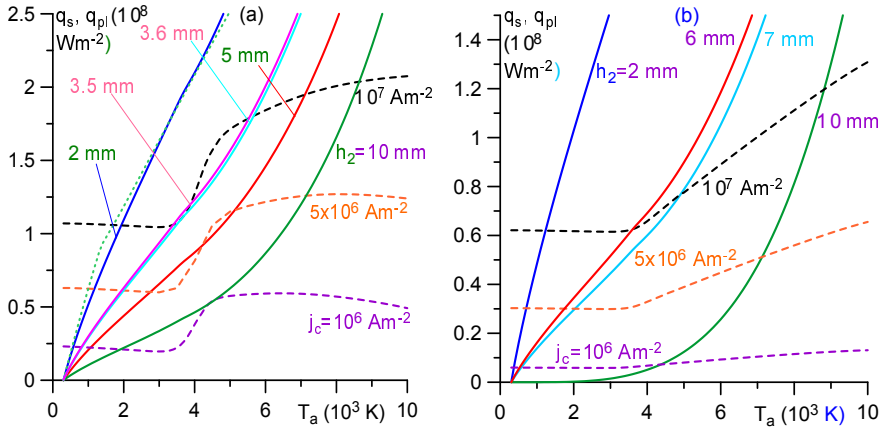

Figure 3. Solid: the energy flux removed by heat conduction from the surface into the anode, q_s, vs. the anode surface temperature T_a for different values of the anode height h_2. Dashed: the energy flux from the plasma to the anode surface, q_{pl}, vs. T_a for different values of the arc length, $h = 0.1$ mm (a) and $h = 10$ mm (b), and for different values of the current density j_c. Very high values of T_a are shown to illustrate the global pattern, although the modelling may be far from reality for states with T_a above the boiling point.

stationary states of the arc and the anode are given by the intersections of the corresponding solid and dashed lines in the Fig. 3. Let us consider, as an example, intersections of the dashed line for $j_c = 10^7$ A m^{-2} in Fig. 3(a). There is one intersection with the solid line for $h_2 = 2$ mm, which corresponds to a stationary state with $T_a = 1900$ K. There are three intersection with the solid line for $h_2 = 3.5$ mm, which correspond to three stationary states possible. Thus, thermal balance of the anode is non-unique in this case. The state where anode surface temperature is the lowest corresponds to $T_a = 3500$ K and it is this state that is achieved in the non-stationary simulations, which shown in the Fig. 2(a) and describe the ignition of a discharge on the cold electrodes in the cold gas.

There is one intersection with the solid line for $h_2 = 3.6$ mm. This intersection corresponds to a stationary state with the computed anode surface temperature $T_a = 5750$ K; the same value which is seen in Fig. 2(a) as it should. [It may seem from the Fig. 3(a) that, in addition to this intersection, there is a tangent point at $T_a \approx 4000$ K, however this is not the case: the tangent point occurs for a slightly lower value of h_2.] There is one intersection with the solid line for $h_2 = 5$ mm, which corresponds to a stationary state with the computed anode surface temperature of 6900 K, again in agreement with the Fig. 2(a).

Thus, the above-described dramatic increase of the computed anode surface temperature, seen in 2(a) as h_2 is increased from 3.5 to 3.6 mm, has a clear graphic interpretation: it stems from the existence of a tangent point of the curve $q_{pl}\,(T_a)$ for $j = 10^7$ A m^2 and the curve $q_s\,(T_a)$ for an h_2 value intermediate between 3.5 and 3.6 mm.

There is one intersection of each solid line and each dashed line in the Fig. 3(b). Hence, thermal balance of the anode is always unique for $h = 10$ mm. No tangent points exist. However, there still is a range of parameters where the intersection of a solid line and a dashed line occurs

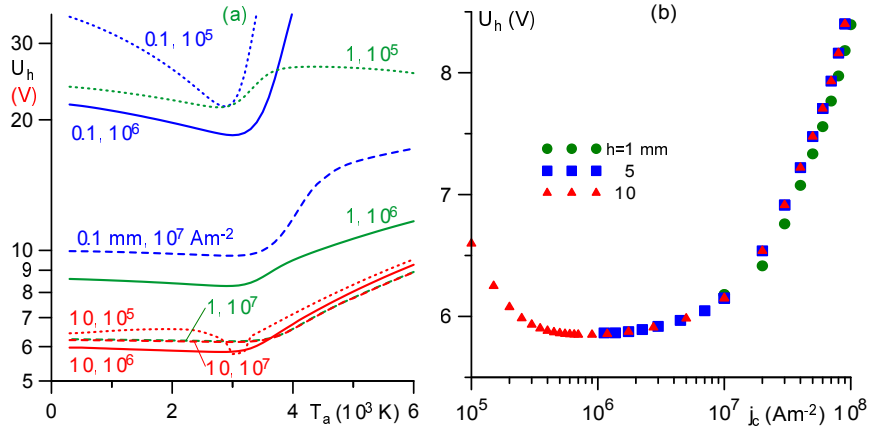

Figure 4. (a) The anode heating voltage vs. the anode surface temperature T_a for different values of the arc length h and the current density j_c. (b) The anode heating voltage vs. the current density for $T_a = 3000\,\mathrm{K}$ and different values of the arc length for conditions where the plasma in the arc bulk is close to LTE.

at a very small angle, as seen in the case $j_c = 10^7\,\mathrm{A\,m^{-2}}$ and $h_2 = 6\,\mathrm{mm}$. A small variation of h_2 in this range of parameters causes a significant change of T_a, e.g., from 3500 K for $h_2 = 6\,\mathrm{mm}$ to 4900 K for $h_2 = 7\,\mathrm{mm}$.

5 Passive anode regime

Two different regimes of heating the anode by the plasma are seen in the Fig. 3, and it is these two regimes that lead to the above-described sharp increase of the computed temperature of the anode surface. In the first regime, which occurs for T_a up to 3000 K or slightly higher, q_{pl} depends on T_a relatively weakly. It is natural to expect that this is the regime of "passive anode", described in the Introduction and associated with the Eq. (1). In the second regime, which occurs for higher T_a, q_{pl} increases with increasing T_a. (The increase subsequently gives way to a decrease for $h = 0.1\,\mathrm{mm}$, $j_c = 10^6$ and $5 \times 10^6\,\mathrm{A\,m^{-2}}$.) This second regime may be called the "active anode" regime.

The passive anode regime is illustrated by the Fig. 4(a). In this figure, the data on q_{pl} for several values of h and j_c are plotted in the form of anode heating voltage, $U_h = q_{pl}/j_c$. For $h = 10\,\mathrm{mm}$, U_h is virtually independent of both the anode surface temperature and the current density in the range $T_a \lesssim 3000\,\mathrm{K}$. A dependence on j_c appears for $h = 1\,\mathrm{mm}$: while the line representing U_h for $j_c = 10^7\,\mathrm{A\,m^{-2}}$ in the Fig. 4(a) for $h = 1\,\mathrm{mm}$ is indistinguishable from the corresponding line for $h = 10\,\mathrm{mm}$, U_h takes higher values for $j_c = 10^6\,\mathrm{A\,m^{-2}}$ and still higher values for $10^5\,\mathrm{A\,m^{-2}}$. Moreover, U_h for $h = 1\,\mathrm{mm}$ and $j_c = 10^6\,\mathrm{A\,m^{-2}}$ and $10^5\,\mathrm{A\,m^{-2}}$ slightly varies with T_a even in the range $T_a \lesssim 3000\,\mathrm{K}$. Values for $h = 0.1\,\mathrm{mm}$ follow the same trend and are still higher.

It is natural to use Eq. (2) with values of the anode heating voltage shown in the Fig. 4(a), or similar, as a boundary condition for multidimensional MHD modelling of high-pressure

	$j_c = 10^5\,\mathrm{A\,m^{-2}}$		$j_c = 10^6\,\mathrm{A\,m^{-2}}$		$j_c = 10^7\,\mathrm{A\,m^{-2}}$	
	IE	TE	IE	TE	IE	TE
$h = 1\,\mathrm{mm}$	-	-	-	$[0.23, 0.71]$	$[0.090, 0.78]$	$[0.10, 0.82]$
$h = 5\,\mathrm{mm}$	-	$[0.52, 3.7]$	$[0.17, 3.7]$	$[0.19, 3.9]$	$[0.073, 4.7]$	$[0.093, 4.8]$
$h = 10\,\mathrm{mm}$	$[0.37, 4.9]$	$[0.49, 7.9]$	$[0.16, 9.1]$	$[0.18, 8.7]$	$[0.073, 9.8]$	$[0.093, 9.8]$

Table 1. Regions of ionization equilibrium (IE) and thermal equilibrium (TE) for different values of the arc length h and the current density j_c.

arc discharges in the approximation of local thermodynamic equilibrium (LTE). Then the first step is to identify, in the entire range of parameters shown in the Fig. 4(a), such conditions under which the plasma in the arc volume is close to LTE. In this connection, Table 1 shows, for different values of the arc length h and the current density j_c, the intervals of x (in mm) where the ionization equilibrium (IE) and thermal equilibrium (TE) hold. The criterion for the ionization equilibrium is that the charged particle density deviates from the equilibrium (Saha) value by no more than 50%, the criterion for the thermal equilibrium is that the electron temperature deviates from the the heavy-particle temperature by no more than 10%. (The criterion for IE is set softer, since the density of the charged particles varies by orders of magnitude.) The LTE amounts to both IE and TE holding simultaneously. One can see that for long arcs, $h \gtrsim 10\,\mathrm{mm}$, the assumption of LTE in the arc bulk is reasonably accurate in the entire current density range $j_c \gtrsim 10^5\,\mathrm{A\,m^{-2}}$. For $h = 5$ and 1 mm, the assumption of LTE in the arc bulk holds starting from j_c of approximately 10^6 and $10^7\,\mathrm{A\,m^{-2}}$, respectively. Note that for $h = 0.1\,\mathrm{mm}$ the LTE is absent even for $j_c = 10^7\,\mathrm{A\,m^{-2}}$.

The values of U_h for the conditions where the LTE in the bulk is present are shown in Fig. 4(b) for three values of the arc length. The dependence on the anode surface temperature is quite weak for these conditions; note for definiteness that the values shown in Fig. 4(b) refer to $T_a = 3000\,\mathrm{K}$. One can see that U_h is virtually independent of the arc length h; a very useful feature that allows one to directly use the data shown in Fig. 4(b), which have been obtained from the 1D modelling of a parallel-plate discharge, for multidimensional MHD LTE modelling of high-pressure arc discharges in configurations of practical interest. U_h weakly varies with the current density j_c, between approximately 6 and 8.5 V for j_c varying over the range from 10^5 to $10^8\,\mathrm{A\,m^{-2}}$.

The data shown in Fig. 4 were computed for a calculation domain that included, in addition to an arc of the length h, also a tungsten cathode of 10 mm height. For $h = 10\,\mathrm{mm}$, the surface temperature T_c of the cathode varied from 2320 K for $j_c = 10^5\,\mathrm{A\,m^{-2}}$ to 4310 K for $j_c = 10^8\,\mathrm{A\,m^{-2}}$. For a different cathode design, values of T_c will be different. However, it is expected that the effect of varying T_c on U_h will be weak if the arc bulk plasma is close to LTE, so there is no direct interaction between the near-cathode and near-anode layers. In order to check this hypothesis, additional calculations have been performed for $h = 10\,\mathrm{mm}$ with both electrodes excluded from the calculation domain, $T_a = 3000\,\mathrm{K}$, and T_c varying over the range $[2300\,\mathrm{K}, 4300\,\mathrm{K}]$. No variation of U_h with T_c was found for $j_c = 10^8$, 10^7, and $10^6\,\mathrm{A\,m^{-2}}$. Note that the calculations for $j_c = 10^8\,\mathrm{A\,m^{-2}}$ were limited to $T_c \geq 3800\,\mathrm{K}$, since at lower T_c the arc voltage rose to values over hundred volts, so the power input was abnormally high and such discharge could not be realized. There was some variation for $j_c = 10^5\,\mathrm{A\,m^{-2}}$, when the LTE region is rather narrow, however it was weak: U_h varied from 6.60 V for $T_c = 2300\,\mathrm{K}$ to 6.06 V for $T_c = 4300\,\mathrm{K}$. Thus, one can expect that the data shown in Fig. 4(b) can be used for arc cathodes of practical interest regardless of details of their design.

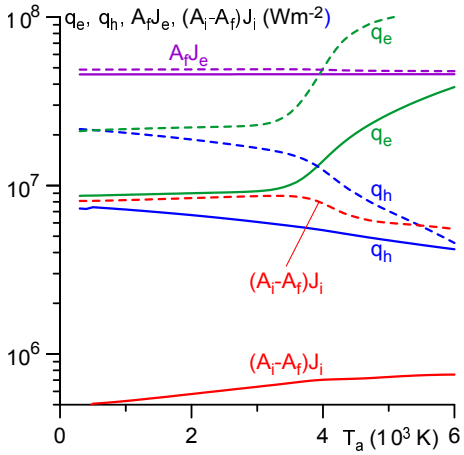

Figure 5. Components of the energy flux to the anode surface vs. the anode surface temperature. q_e, q_h: fluxes of thermal energy of the electrons and the heavy particles. $A_f J_e$: the electron condensation heat. $(A_i - A_f)J_i$: the energy released at the anode due to the neutralization of the ions. $j_c = 10^7\,\mathrm{A\,m^{-2}}$. Solid: $h = 10\,\mathrm{mm}$. Dashed: $h = 0.1\,\mathrm{mm}$.

In summary, Eq. (2) with the values of the anode heating voltage shown in the Fig. 4(b) can be used as a boundary condition for multidimensional MHD LTE modelling of high-pressure arc discharges under all conditions where the LTE modelling approach as such is justified, that is, in the case when the arc length and current are high enough so that the plasma in the arc bulk is close to LTE. Note that, taking into account the weak variation of U_h with the cathode surface temperature for $j_c = 10^5\,\mathrm{A\,m^{-2}}$, described in the preceding paragraph, the anode heating voltage U_h in the range $j_c \lesssim 10^6$ in Fig. 4 may be set constant at a value around 6 V. This result agrees very well with values of the anode heating voltage of $6.1 - 6.2\,\mathrm{V}$, found in the experiment [4, 17] and simulations [18].

For short arcs and/or low arc currents, LTE modelling approaches are unjustified and it makes no sense to consider the corresponding U_h values, shown in Fig. 4(a), for eventual boundary conditions. However, the values by itself remain valid, since they have been obtained by a fully non-equilibrium modelling of the entire arc up to the electrode surfaces. Note that the anode heating voltage offers a convenient form of representation of calculated values of the density of energy flux to the surface of arc anodes, regardless of the presence or absence of any kind of equilibrium in the bulk plasma.

The components of the energy flux from the plasma to the anode surface, i.e., the terms of the rhs of the second expression in Eq. (9) evaluated at the anode surface, are shown in the Fig. 5. The energy transported to the anode surface by thermal conduction of the heavy particles is negligible. This is in contrast to what happens at the cathode surface, where the thermal conduction of heavy particles makes the greatest contribution to the energy transfer [29, 50]. The energy released at the anode surface due to the neutralization of the ions is small as well, meaning that the ion current to the anode is small as expected.

Since $J_e \approx j_c/e$, the electron condensation heat $A_f J_e$ is close to $4.5\times10^7\,\mathrm{W\,m^{-2}}$ and virtually

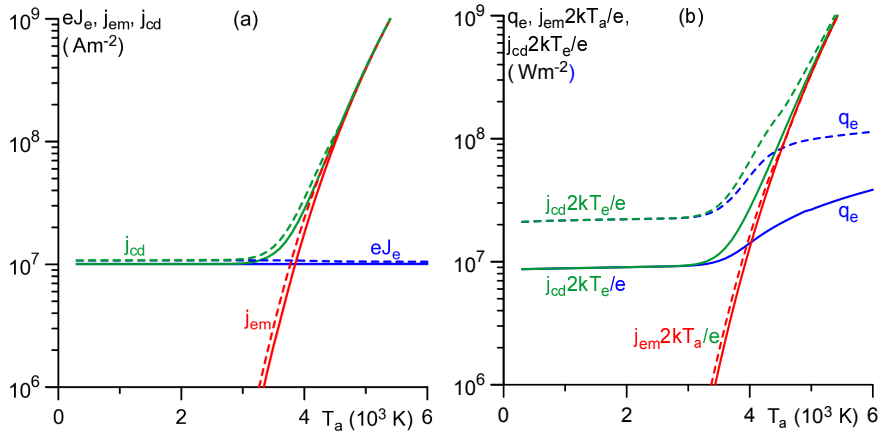

Figure 6. (a): balance of the electron fluxes at the anode surface; cf. equation (3). (b): balance of the electron energy fluxes at the anode surface; cf. equation (5). $j_c = 10^7\,\mathrm{A\,m^{-2}}$. Solid: $h = 10\,\mathrm{mm}$. Dashed: $h = 0.1\,\mathrm{mm}$.

independent of parameters. The contribution of this term to the anode heating voltage is $A_f/e = 4.5\,\mathrm{V}$. For $h = 10\,\mathrm{mm}$ this constitutes the main component of the total anode heating voltage in the passive regime, which is about 6 V. For $h = 0.1\,\mathrm{mm}$, other components of the energy flux are larger than for $h = 10\,\mathrm{mm}$, and their combined contribution is comparable to $A_f J_e$, therefore the total heating voltage in the passive regime is approximately twice A_f/e.

6 Active anode regime

It is also seen in the Fig. 5 that, as T_a exceeds values around 3000 K or somewhat higher, q_e the density of flux of thermal energy of the electrons to the anode begins to increase. This causes an increase in q_{pl} the total energy flux from the plasma to the anode surface: the active regime occurs.

Balance of the electron particle fluxes and the electron energy fluxes at the anode surface for different values of the anode temperature is shown in the Fig. 6; cf. Eqs. (3) and (5). It is seen from the Fig. 6(a) that for low anode temperatures, where the thermionic electron emission is negligible, the current transport to the anode is ensured by the flux of the electrons coming to the anode surface from the plasma: $j_{cd} \approx eJ_e \approx j_c$. The electron thermionic emission comes into play at T_a around 3000 K and rapidly overtakes the net electron current, so that the thermionic electron emission is balanced by the current of electrons coming to the anode surface from the plasma: $j_{cd} \approx j_{em} \gg j_c$.

A similar behavior is revealed by components of the electron energy flux shown in Fig. 6(b). For $T_a \lesssim 3000\,\mathrm{K}$, the electron energy transport to the anode is ensured by the energy flux of the electrons coming to the anode surface from the plasma, $q_e \approx j_c 2kT_e/e$, and is virtually independent of T_a. For increasing T_a, the electron emission energy flux comes into play at T_a around 3000 K and then rapidly overtakes the net electron thermal energy flux q_e (which starts increasing as well, however much slower, as was already seen in the Fig. 5), so the electron

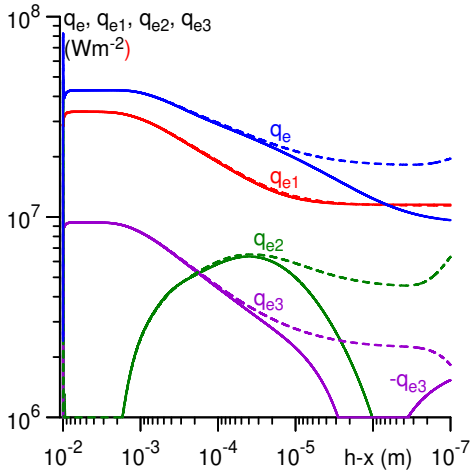

Figure 7. Distributions in the arc of the density of the electron thermal energy flux and of its components. $h-x$: the distance from the anode. q_e: the density of the electron thermal energy flux. q_{e1}, q_{e2}, q_{e3}: components of q_e due to, respectively, the enthalpy transport by the electron transport flux, the electron heat conduction, and the effect inverse to the thermal diffusion. $j_c = 10^7\,\mathrm{A\,m^{-2}}$. $h = 10\,\mathrm{mm}$. Solid: $T_a = 3000\,\mathrm{K}$. Dashed: $T_a = 5000\,\mathrm{K}$.

emission energy flux is balanced by the energy flux transported by the electrons coming to the anode surface from the plasma: $j_{cd}2kT_e/e \approx j_{em}2kT_a/e \gg q_e$.

The Fig. 6, while being interesting and illustrative, does not explain why the net electron thermal energy flux q_e starts increasing with increasing T_a, thus originating the active anode regime. The governing process should be sought somewhere else. An example of the distribution in the arc of the density of the net electron thermal energy flux and its components, i.e., the terms of the Eq. (6), is shown in Fig. 7. Note that the lines depicting the enthalpy transport by the electron transport flux, q_{e1}, for $T_a = 3000\,\mathrm{K}$ and $T_a = 5000\,\mathrm{K}$ are virtually indistinguishable.The electron thermal energy fluxes due to the heat conduction and the effect inverse to the thermal diffusion, q_{e2} and q_{e3}, remain positive (directed to the anode) for $T_a = 5000\,\mathrm{K}$, but turn negative in the vicinity of the anode for $T_a = 3000\,\mathrm{K}$, the reasons being, respectively, a small increase of T_e in the direction to the anode and a change of sign in one of the kinetic coefficient governing q_{e3} [$A_a^{(e)}$ in Eq. (15) of [22]].

At distances from the anode exceeding approximately $30\,\mu\mathrm{m}$, the net electron energy fluxes q_e for $T_a = 3000\,\mathrm{K}$ and $T_a = 5000\,\mathrm{K}$ virtually coincide. A difference appears for smaller distances and then increases; it equals $0.78 \times 10^7\,\mathrm{W\,m^{-2}}$ at the point $h - x = 0.3\,\mu\mathrm{m}$, which is approximately where the dependence $q_e\,(x)$ for $T_a = 5000\,\mathrm{K}$ takes a minimum, and $1.72 \times 10^7\,\mathrm{W\,m^{-2}}$ at the anode surface. (Note for definiteness that the values of the function $q_e\,(x)$ for $T_a = 3000\,\mathrm{K}$ are $1.04\times10^7\,\mathrm{W\,m^{-2}}$ at the point $h-x = 0.3\,\mu\mathrm{m}$ and $0.93\times10^7\,\mathrm{W\,m^{-2}}$ at the anode surface; the corresponding values for $T_a = 5000\,\mathrm{K}$ are 1.82×10^7 and $2.65 \times 10^7\,\mathrm{W\,m^{-2}}$.) One can say that about 50% of the difference in the electron fluxes to the anode surface between the cases of active anode, $T_a = 5000\,\mathrm{K}$, and passive anode, $T_a = 3000\,\mathrm{K}$, is accumulated in the region $0.3\,\mu\mathrm{m} \lesssim h - x \lesssim 30\,\mu\mathrm{m}$ and the rest is accumulated in the immediate vicinity

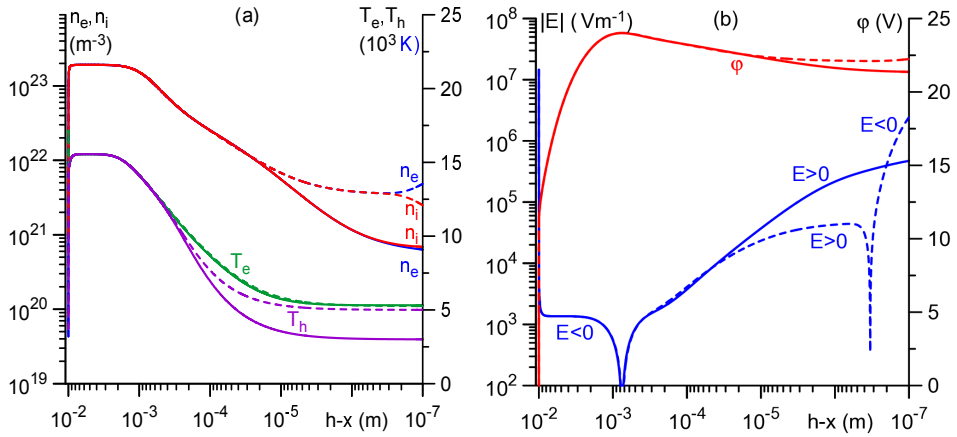

Figure 8. Distributions of parameters in the arc. (a): the ion and electron densities and the electron and heavy-particle temperatures. (b): The electric field and the electrostatic potential. $h - x$: the distance from the anode. $j_c = 10^7\,\mathrm{A\,m^{-2}}$, $h = 10\,\mathrm{mm}$. Solid: $T_a = 3000\,\mathrm{K}$. Dashed: $T_a = 5000\,\mathrm{K}$.

of the anode, $h - x \lesssim 0.3\,\mu\mathrm{m}$. Note that this result should be viewed with caution, since hydrodynamics equations do not represent a good approximation on submicron length scales; additional comments on this point will follow.

In order to understand these effects, let us consider the distributions of parameters in the arc, shown in Fig. 8. Note that the lines depicting the electron temperature T_e distributions for $T_a = 3000\,\mathrm{K}$ and $T_a = 5000\,\mathrm{K}$ are virtually indistinguishable in the Fig. 8(a). There is an increase in T_e in the vicinity of the anode in the case $T_a = 3000\,\mathrm{K}$, but it is very small and is not visible on the graph. Also virtually indistinguishable are distributions of the ion and electron number densities n_i and n_e in the case $T_a = 3000\,\mathrm{K}$: the near-anode space-charge sheath is virtually inexistent in this case. There is a pronounced negative near-anode space-charge sheath in the case $T_a = 5000\,\mathrm{K}$, positioned within approximately $0.3\,\mu\mathrm{m}$ from the anode. The electric field, shown in Fig. 8(b), is directed to the cathode, $E < 0$, in the near-cathode region and the bulk of the arc. There is a field reversal at 0.75 mm from the anode, after which E remains positive up to the anode surface in the case $T_a = 3000\,\mathrm{K}$. In the case $T_a = 5000\,\mathrm{K}$, the electric field changes its direction once again and is negative within the near-anode space-charge sheath, $h - x \lesssim 0.3\,\mu\mathrm{m}$. The near-anode voltage drop is negative for $T_a = 3000\,\mathrm{K}$, i.e., in the passive anode regime, and slightly positive for $T_a = 5000\,\mathrm{K}$, in the active regime.

Distributions of plasma parameters, shown in the Fig. 8, are unaffected by T_a in the most part of the arc, however there is a pronounced effect within approximately $30\,\mu\mathrm{m}$ from the anode. In particular, the charged particle densities for $T_a = 5000\,\mathrm{K}$ are several times higher than for $T_a = 3000\,\mathrm{K}$, which is due to the effect of the thermionic electron emission from the anode. This causes an increase in the electron thermal conductivity κ_e, as seen in Fig. 9. (Note that κ_e is determined in this work by Eqs. (50)-(53) of [22] and is a rather complex function of plasma parameters, in the first place, n_e and T_e; the dependence $\kappa_e\,(n_e)$ is, unsurprisingly, increasing.) In turn, an increase in κ_e results in an increase of the electron thermal conduction flux from the bulk plasma to the near-anode layer; cf. the solid and dashed lines depicting q_{e2}

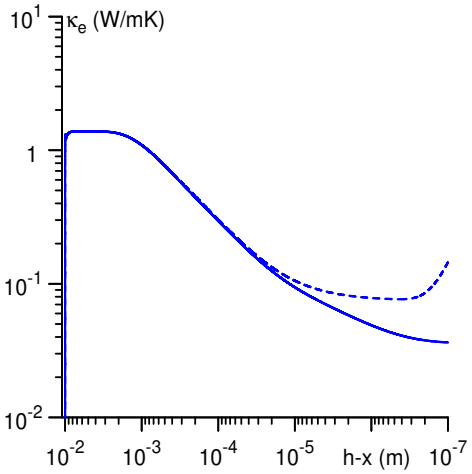

Figure 9. Distribution of the electron thermal conductivity. $j_c = 10^7\,\mathrm{A\,m^{-2}}$. $h = 10\,\mathrm{mm}$. Solid: $T_a = 3000\,\mathrm{K}$. Dashed: $T_a = 5000\,\mathrm{K}$.

in Fig. 7. This explains the higher values of the net electron thermal energy flux q_e on distances between 30 and $0.3\,\mu$m from the anode in the active regime compared to the passive regime.

The point of minimum of the dependence $q_e\,(x)$ in the active regime case, $h - x \approx 0.3\,\mu$m, mentioned above, approximately coincides with the edge of the near-anode space-charge sheath, so the increase of the dependence $q_e\,(x)$ within $0.3\,\mu$m from the anode in the case $T_a = 5000\,\mathrm{K}$, seen in the Fig. 7, is due to the heating of the electron gas by the sheath electric field. Note that in framework of the hydrodynamics model being used, the energy received by the electron gas from the sheath electric field is transported to the anode by the electron heat conduction, as shown by the increase of the dependence $q_{e2}\,(x)$ for $T_a = 5000\,\mathrm{K}$ in the region $h - x \lesssim 0.3\,\mu$m, seen in in Fig. 7. However, this conclusion cannot be trusted since hydrodynamics equations do not represent a good approximation on submicron length scales. On the other hand, the equation of conservation of energy of the electrons, Eq. (19) of [36], remains valid regardless of length scales, hence the computed dependence $q_e\,(x)$ should be at least qualitatively correct.

Thus, the bottom reason of the active anode regime is the thermionic electron emission from the anode, coming into play as T_a attains values of 3000 K or somewhat higher. The emission does not affect significantly the current transfer, since most of the emitted electrons return to the anode as shown by Fig. 6(a). However, it causes a significant increase in the electron density near the anode, which causes two effects resulting in increase of the total energy flux from the plasma to the anode. One effect is an increase in the electron thermal conductivity near the anode, which in turn results in an increase of the electron thermal conduction flux from the bulk plasma to the near-anode layer. The other effect that gives a comparable contribution is the formation of a negative near-anode space-charge sheath with a positive voltage drop, which results in heating of the electron gas by the sheath electric field.

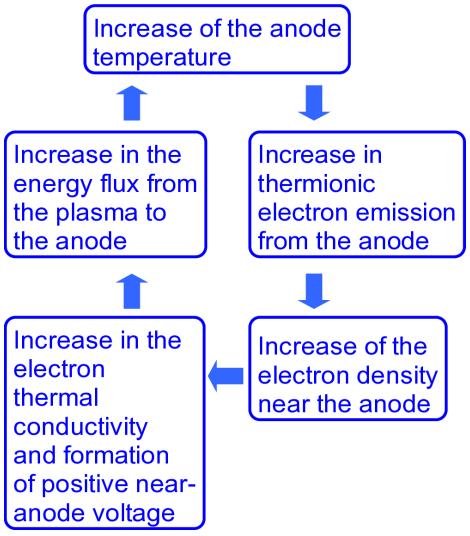

Figure 10. Mechanism of thermal instability in the anodes of high-pressure high-current arc discharges.

7 Thermal instability in the anode

The increasing dependence of the energy flux q_{pl} from the plasma to the anode on the temperature of the anode surface T_a represents a positive feedback that can cause thermal instability: an increase in T_a affects processes in the plasma and, in particular, causes an increase in the energy flux q_{pl} from the plasma to the anode; the increased energy input to the anode causes a further increase in the anode temperature T_a, *etc.* This mechanism is illustrated by Fig. 10. A similar thermal instability with feedback of a different nature (unrelated to the electron energy flux to the electrode surface) is known to occur on thermionic arc cathodes and results in appearance of cathode spot; e.g., review [2] and references therein.

The occurrence of the active regime in non-stationary simulations occurs via the development of this instability, as shown in Sec. 3 (see discussion of the Fig. 2(a)). Analysis of stability of stationary states against this instability may be carried out along the lines of the analytic theory of stability of direct current transfer to thermionic cathodes [51] and is skipped for brevity. The result is as follows: a stationary state is stable if the inequality $\partial q_s/\partial T_a > \partial q_{pl}/\partial T_a$ is satisfied for the T_a value corresponding to this state, and unstable otherwise. The physical meaning of this result is clear: for a stationary state to be stable against a thermal instability, the heat removal by thermal conduction and by the thermal radiation, which produces a stabilizing effect, should be intensive enough. Note that their derivative $\partial q_s/\partial T_a$, evaluated in the quasi-stationary approximation, is given by $\partial q_s/\partial T_a = \kappa_s\left(T_a\right)/h_2 + \sigma\, T_a^3\left(4\varepsilon + T_a\, d\varepsilon/dT_a\right)$.

It is seen from Fig. 2 that, if only one stationary state is possible, then the slope of the solid line at the intersection exceeds the slope of the dashed line, hence the above inequality holds and this state is stable. Such states can be computed by means of non-stationary simulations, similar to the ones shown in the Fig. 2(a) and describing the ignition of a discharge on the cold electrodes in a cold gas. In principle, such states may be realized in experiment, unless T_a

exceeds the boiling temperature.

If three stationary states are possible, as in the cases $j_c = 10^7\,\mathrm{A\,m^{-2}}$ and $h_2 = 3.5\,\mathrm{mm}$, or $j_c = 5 \times 10^6\,\mathrm{A\,m^{-2}}$ and $h_2 = 5\,\mathrm{mm}$, or $j_c = 10^6\,\mathrm{A\,m^{-2}}$ and $h_2 = 10\,\mathrm{mm}$ in the Fig. 3(a), then the above inequality is satisfied in the states with the lowest and the highest temperatures. Hence, such states are stable and can be computed by means of non-stationary simulations. In particular, the state with lowest temperature for $h_2 = 3.5\,\mathrm{mm}$, which is $T_a = 3500\,\mathrm{K}$ (for $j_c = 10^7\,\mathrm{A\,m^{-2}}$ and the arc length $h = 100\,\mu\mathrm{m}$), is attained in the non-stationary simulation shown in the Fig. 2(a). Note that the latter simulation describes the discharge ignition on cold electrodes in the cold gas. A different initial condition, the one with a hot anode, may be needed to obtain the other stable solution (the one with the highest anode surface temperature). Stationary states with the intermediate temperature value are unstable.

8 Conclusions

Two regimes of current transfer to the anodes of high-pressure high-current arc discharges have been investigated by means of the unified numerical modelling. In the first regime, which occurs for low and moderate anode surface temperatures T_a, the energy flux from the plasma to the anode surface, q_{pl}, depends on T_a relatively weakly; see Figs. 3, 5, and 6(b). This regime is associated with the Eqs. (1) and (2) and may be termed the "passive anode" regime.

There is another regime, in which q_{pl} varies with T_a and is higher than in the passive anode regime. This regime may be called the "active anode" regime. It occurs as T_a exceeds approximately 3000 K and stems from the thermionic electron emission from the anode coming into play. The emission does not appreciably affect the current transfer, since most of the emitted electrons return to the anode. However, the emission causes a significant increase in the electron density near the anode, which causes two effects resulting in increase of the total energy flux from the plasma to the anode, q_{pl}. One effect is an increase of the electron energy transport from the bulk plasma to the near-anode layer by electron heat conduction. The other effect, that gives a comparable contribution, is the formation of a negative near-anode space-charge sheath with a positive voltage drop, which results in heating of the electron gas by the sheath electric field.

It should be stressed that the evaporation cooling may play a role in the thermal balance of the anode at temperatures above the boiling point. Therefore, computation results on the well-developed active regime are at best qualitatively correct. On the other hand, surface temperatures above the boiling point will cause a fast destruction of the electrode if they occur in the experiment, and in this sense qualitative results are sufficient for practice.

The increasing dependence of the energy flux q_{pl} from the plasma to the anode on the temperature of the anode surface T_a represents a positive feedback. This feedback can cause a thermal instability, which is illustrated by the Fig. 10. Apart from the nature of a feedback, this is the same thermal instability that occurs on thermionic arc cathodes and results in appearance of cathode spots. The emergence of the active regime in non-stationary simulations occurs via the development of this instability, as seen in the Fig. 2(a).

Eq. (2) with the values of the anode heating voltage U_h shown in the Fig. 4(b) can be used as a boundary condition for multidimensional MHD LTE modelling of high-pressure arc discharges under all conditions where the LTE modelling approach as such is justified, that is, in the case when the arc length and current are high enough so that the plasma in the arc bulk is close to LTE. The value of U_h is independent of the arc length and of the cathode surface

temperature, although it weakly varies with the current density j_c, between approximately 6 and 8.5 V for j_c in the range from 10^5 to 10^8 A m^{-2}.

For short arcs and/or low arc currents, LTE modelling approaches are unjustified and there is no sense in using corresponding values of U_h, shown in Fig. 4(a), for boundary conditions. However, the values by itself remain valid, since they have been obtained by a fully non-equilibrium modelling of the entire arc up to the electrode surfaces. Note that since U_h characterizes only the plasma side, in can be useful not only for the passive regime, but also for the beginning of the active regime, while the anode temperature has not reached the boiling point.

The active anode regime may occur on hot refractory anodes, an example being electrodes of high-intensity discharge lamps, where a high anode temperature is desirable to avoid the formation of high re-ignition peaks at the beginning of the cathodic phase. The occurrence of the active regime is strongly affected by parameters, in particular, by the distance h_2 between the anode surface and the cooling fluid, and the local current density j_c, which is conveniently illustrated by the graphic representation in the Fig. 3. It is interesting to note that an increase in h_2 causes, somehow counterintuitively, an increase in the arc voltage as seen in Fig. 2(a).

Acknowledgments The work at Universidade da Madeira was supported by FCT - Fundação para a Ciência e a Tecnologia of Portugal under project UIDP/50010/2020 and by European Regional Development Fund through the Operational Program of the Autonomous Region of Madeira 2014-2020 under project PlasMa-M1420-01-0145-FEDER-000016.

Data availability

The data that support the findings of this study are available from the corresponding author upon reasonable request.

A Cooling of the electrode surface by evaporation of the electrode material

As mentioned in Sec. 2, the condition of continuity of the energy flux at the electrode surface, Eq. (8), does not account for the cooling of the electrode surface by evaporation of the electrode material. Let us estimate this effect. Let J_v be the density of flux of atoms evaporated from the electrode surface. Note that J_v is usually estimated by means of the Langmuir formula: $J_v = p_v \left(2\pi m_v k T_w\right)^{-1/2}$, where T_w is the electrode surface temperature, p_v is the pressure of the saturated vapor of the electrode material evaluated at the temperature T_w, and m_v is the electrode metal atom mass. Some of the evaporated atoms undergo one or more collisions with atoms of the background (plasma-producing) gas near the surface and are reflected back to the surface. Therefore, the net flux of the vapor from the surface into the plasma is always lower than J_v.

If p_v does not exceed the pressure p_{amb} of the ambient gas, then most of the evaporated atoms are reflected back to the surface and the net flux of the vapor from the surface is governed by the removal of the vapor from the surface due to diffusion of the vapor into the bulk of the ambient gas [38]. Therefore, the net vapor flux is smaller than J_v by a factor of the order of the Knudsen number λ/L, where λ is the mean free path of the vapor atoms in the ambient gas and L is a characteristic dimension of the arc.

The contribution of the evaporation cooling to the energy balance of the electrode surface may be characterized by the ratio

$$R = \frac{(\lambda/L)\, J_v A_v}{(j_c/e)\, A_f}, \tag{A1}$$

where A_v is the evaporation energy per atom. Note that the quantity in the numerator is an order-of-magnitude estimate of the evaporation cooling and $(j/e)\,A_f$ is the cooling or heating of the electrode surface by, respectively, emission or condensation of the electrons.

The mean free path λ may be expressed as $\lambda = 1/n_a\sigma$, where n_a is the number density of atoms of the plasma-producing gas (argon) at the electrode surface and σ is the momentum-transfer cross section for collisions of the vapor atoms with atoms of the plasma-producing gas. n_a may be estimated by order of magnitude as $n_a = p_{amb}/kT_w$. Substituting these expressions and the Langmuir formula, one can rewrite Eq. (A1) in a form convenient for rapid evaluations:

$$R = R_1\sqrt{\frac{T_w}{T_b}}\frac{p_v}{p_{amb}}, \quad R_1 = \frac{R_2}{j_c L}, \quad R_2 = \frac{A_v}{A_f}\frac{e}{\sigma}\left(\frac{kT_b}{2\pi m_v}\right)^{1/2}, \tag{A2}$$

where T_b is the boiling temperature.

Assuming $\sigma = 10^{-19}\,\mathrm{m}^2$, one finds that $R_2 = 582\,\mathrm{A/m}$ for tungsten ($m_v = 184\,\mathrm{u}$, $T_b = 5830\,\mathrm{K}$, $A_v = 7.98\,\mathrm{eV}$) and $R_2 = 272\,\mathrm{A/m}$ for copper ($m_v = 64\,\mathrm{u}$, $T_b = 2835\,\mathrm{K}$, $A_v = 3.15\,\mathrm{eV}$). For the the current density $j_c = 10^6\,\mathrm{A\,m^{-2}}$ and the arc length $L = 1\,\mathrm{mm}$, one finds $R_1 = 0.58$ for tungsten and $R_1 = 0.27$ for copper.

It follows that for atmospheric-pressure arcs, $p_{amb} = 1\,\mathrm{atm}$, when the electrode surface temperature is at the boiling point, $T_w = T_b$, and the pressure of the saturated vapor is atmospheric, $p_v = 1\,\mathrm{atm}$, R is comparable to unity: $R = 0.58$ for tungsten and $R = 0.27$ for copper. For lower temperatures, R is much smaller than unity. For example, p_v for tungsten at $T_w = 4000\,\mathrm{K}$, evaluated with the use of the data [48], is 0.49 mbar, thus $R = 2.4\times10^{-4}$; p_v for copper at $T_w = 2000\,\mathrm{K}$, evaluated with the use of the data [52], is 4.4 mbar, thus $R = 10^{-3}$.

One can conclude that the contribution of the evaporation cooling to the energy balance of the surfaces of electrodes of atmospheric-pressure arcs is small if the temperature of the surface is below the boiling temperatures, however the evaporation cooling may become appreciable for higher temperatures, in agreement with the conclusion drawn in [38].

References

[1] A. Gleizes, J. J. Gonzalez, and P. Freton, J. Phys. D: Appl. Phys. **38**, R153 (2005).

[2] M. S. Benilov, J. Phys. D: Appl. Phys. **41**, 144001 (30pp) (2008).

[3] J. Heberlein, J. Mentel, and E. Pfender, J. Phys. D: Appl. Phys. **43**, 023001 (2010).

[4] J. Mentel and J. Heberlein, J. Phys. D: Appl. Phys. **43**, 023002 (2010).

[5] S. M. Shkol'nik, Plasma Sources Sci. Technol. **20**, 013001 (2011).

[6] A. Gleizes, Plasma Chem. Plasma Process. **35**, 455 (2015).

[7] A. B. Murphy, Plasma Chem. Plasma Process. **35**, 471 (2015).

[8] M. I. Boulos, P. Fauchais, and E. Pfender, *Handbook of Thermal Plasmas* (Springer Int. Publishing, Cham, 2016).

[9] C. Chazelas, J. P. Trelles, I. Choquet, and A. Vardelle, Plasma Chem. Plasma Process. **37**, 627 (2017).

[10] A. B. Murphy and D. Uhrlandt, Plasma Sources Sci. Technol. **27**, 063001 (2018).

[11] I. Choquet, Welding in the World **62**, 177 (2018).

[12] M. S. Benilov, J. Phys. D: Appl. Phys. **53**, 013002 (2020).

[13] H. A. Dinulescu and E. Pfender, J. Appl. Phys. **51**, 3149 (1980).

[14] V. A. Nemchinsky and Y. Raitses, Plasma Sources Sci. Technol. **25**, 035003 (2016).

[15] A. R. Mansour and K. Hara, J. Phys. D: Appl. Phys. **52**, 105204 (2019).

[16] A. Khrabry, I. D. Kaganovich, A. Khodak, V. Vekselman, and T. Huang, J. Appl. Phys. **128**, 123303 (2020).

[17] M. Redwitz, L. Dabringhausen, S. Lichtenberg, O. Langenscheidt, J. Heberlein, and J. Mentel, J. Phys. D: Appl. Phys. **39**, 2160 (2006).

[18] N. A. Almeida, M. D. Cunha, and M. S. Benilov, J. Phys. D: Appl. Phys. **50**, 385203 (2017).

[19] M. Lisnyak, M. D. Cunha, J.-M. Bauchire, and M. S. Benilov, J. Phys. D: Appl. Phys. **50**, 315203 (2017).

[20] M. Tanaka, M. Ushio, and C. S. Wu, J. Phys. D: Appl. Phys. **32**, 605 (1999).

[21] Q. Sun, C. Wang, Z. long Zhang, X. hui Chen, P. Qin, and W.-D. Xia, J. Phys. D: Appl. Phys. **52**, 265204 (2019).

[22] N. A. Almeida, M. S. Benilov, and G. V. Naidis, J. Phys. D: Appl. Phys. **41**, 245201 (26pp) (2008).

[23] N. A. Almeida, M. S. Benilov, U. Hechtfischer, and G. V. Naidis, J. Phys. D: Appl. Phys. **42**, 045210 (11pp) (2009).

[24] S. Kolev and A. Bogaerts, Plasma Sources Sci. Technol. **24**, 015025 (2015).

[25] I. L. Semenov, I. V. Krivtsun, and U. Reisgen, J. Phys. D: Appl. Phys. **49**, 105204 (2016).

[26] A. I. Saifutdinov, I. I. Fairushin, and N. F. Kashapov, JETP Lett. **104**, 180 (2016).

[27] S. I. Eliseev, A. Kudryavtsev, H. Liu, Z. Ning, D. Yu, and A. S. Chirtsov, IEEE Trans. Plasma Sci. **44**, 2536 (2016).

[28] S. Kolev, S. Sun, G. Trenchev, W. Wang, H. Wang, and A. Bogaerts, Plasma Processes Polym. **14**, 1600110 (2017).

[29] A. Khrabry, I. D. Kaganovich, V. Nemchinsky, and A. Khodak, Phys. Plasmas **25**, 013521 (2018).

[30] A. Khrabry, I. D. Kaganovich, V. Nemchinsky, and A. Khodak, Phys. Plasmas **25**, 013522 (2018).

[31] M. Baeva, D. Loffhagen, M. M. Becker, and D. Uhrlandt, Plasma Chem. Plasma Process. **39**, 949 (2019).

[32] M. Baeva, D. Loffhagen, and D. Uhrlandt, Plasma Chem. Plasma Process. **39**, 1359 (2019).

[33] M. Baeva, D. Uhrlandt, and D. Loffhagen, Jap. J. Appl. Phys. **59**, SHHC05 (2020).

[34] M. Baeva, V. F. Boretskij, D. Gonzalez, R. Methling, O. Murmantsev, D. Uhrlandt, and A. Veklich, J. Phys. D Appl. Phys. **54**, 025203 (2020).

[35] M. Baeva, R. Methling, and D. Uhrlandt, Plasma Sci. Technol. **8**, 1 (2021).

[36] D. F. Santos, M. Lisnyak, N. A. Almeida, L. G. Benilova, and M. S. Benilov, J. Phys. D: Appl. Phys. (2021).

[37] M. Baeva, M. Stankov, T. Trautvetter, R. Methling, F. Hempel, D. Loffhagen, and R. Foest, J. Phys. D: Appl. Phys. **54**, 355205 (2021).

[38] M. S. Benilov, S. Jacobsson, A. Kaddani, and S. Zahrai, J. Phys. D: Appl. Phys. **34**, 1993 (2001).

[39] A. J. Shirvan, I. Choquet, and H. Nilsson, J. Phys. D: Appl. Phys. **49**, 485201 (2016).

[40] Yu. P. Raizer, *Gas Discharge Physics* (Springer, Berlin, 1991).

[41] P. Tolias, Nucl. Mater. Energy **13**, 42 (2017).

[42] S. W. H. Yih and C. T. Wang, *Tungsten: Sources, Metallurgy, Properties, and Applications* (Plenum Press, New York, 1979).

[43] H. Kaufmann, *Advanced Modeling of Plasma-Cathode Interaction in Vacuum and Unipolar Arcs,* Ph.D. thesis, Universidade da Madeira, 2019.

[44] Y. S. Touloukian, R. W. Powell, C. Y. Ho, and P. G. Clemens, *Thermal Conductivity. Metallic Elements and Alloys*, *Thermophysical Properties of Matter, vol. 1* (IFI/Plenum, New York-Washington, 1970).

[45] E. A. Estalote and K. G. Ramanathan, J. Opt. Soc. Am. **67**, 39 (1977).

[46] K. G. Ramanathan and S. H. Yen, J. Opt. Soc. Am. **67**, 32 (1977).

[47] H. Masuda and M. Higano, J. Opt. Soc. Am. A **2**, 1877 (1985).

[48] W. F. Gale and T. C. Totemeier, eds., *Smithells Metals Reference Book*, 8th ed., (Elsevier Butterworth-Heinemann, Amsterdam and Boston, 2004).

[49] V. S. Fomenko, *Emission Properties of Materials*, 4th ed. (Naukova Dumka, Kiev, Kiev, 1981), in Russian.

[50] M. S. Benilov, N. A. Almeida, M. Baeva, M. D. Cunha, L. G. Benilova, and D. Uhrlandt, J. Phys. D: Appl. Phys. **49**, 215201 (2016).

[51] M. S. Benilov, J. Phys. D: Appl. Phys. **40**, 1376 (2007).

[52] D. R. Lide, ed., *CRC Handbook of Chemistry and Physics*, 84th ed., (CRC Press, Boca Raton, 2003-2004).